

Nonlinear dynamics in horizontal film boiling

By CHARLES H. PANZARELLA¹, STEPHEN H. DAVIS¹
AND S. GEORGE BANKOFF²

¹Department of Engineering Sciences and Applied Mathematics, Northwestern University,
Evanston, IL 60208, USA

²Department of Chemical Engineering, Northwestern University, Evanston, IL 60208, USA

(Received 1 December 1997 and in revised form 13 August 1999)

This paper uses thin-film asymptotics to show how a thin vapour layer can support a liquid which is heated from below and cooled from above, a process known as horizontal film boiling. This approach leads to a single, strongly-nonlinear evolution equation which incorporates buoyancy, capillary and evaporative effects. The stability of the vapour layer is analysed using a variety of methods for both saturated and subcooled film boiling. In subcooled film boiling, there is a stationary solution, a constant-thickness vapour film, which is determined by a simple heat-conduction balance. This is Rayleigh–Taylor unstable because the heavier liquid is above the vapour, but the instability is completely suppressed for sufficient subcooling. A bifurcation analysis determines a supercritical branch of stable, spatially-periodic solutions when the basic state is no longer stable. Numerical branch tracing extends this into the strongly-nonlinear regime, revealing a hysteresis loop and a secondary bifurcation to a branch of travelling waves which are stable under certain conditions. There are no stationary solutions in saturated film boiling, but the initial development of vapour bubbles is determined by directly solving the time-dependent evolution equation. This yields important information about the transient heat transfer during bubble development.

1. Introduction

Consider film boiling on top of a solid, horizontal heating surface as shown in figure 1. The temperature T'_s of the solid is much greater than the boiling temperature T'_{SAT} , also known as the equilibrium or saturation temperature, and the rapidly evaporating liquid produces a thin vapour film which spreads across the entire heating surface. When this happens, the increased thermal resistance of the vapour significantly reduces the heat transfer. Film boiling is often encountered in the quenching of hot metals, and this reduction in heat transfer can significantly affect the quality of the final product. In addition, the destabilization of film boiling is responsible for steam explosions in the degraded core conditions of a nuclear reactor (cf. Kikuchi, Ebisu & Michiyoshi 1992). These are just two of the many industrial processes which would benefit from a better understanding of the mechanisms responsible for film boiling.

Recent experimental evidence has also shown that pool boiling in microgravity is much different to that on the ground (cf. Ervin *et al.* 1992). The familiar pool boiling curves relating heat flux to surface temperature, which have been determined from ground-based experiments, do not adequately describe the same process in space. In particular, film boiling is observed at a much lower superheat, the vapour bubbles grow

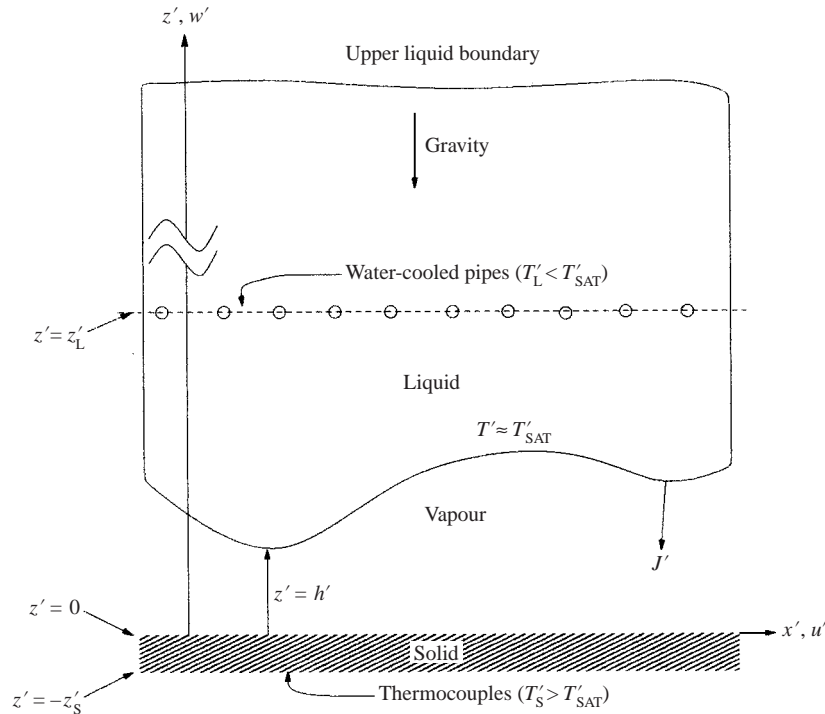


FIGURE 1. The two-dimensional film-boiling model. The vapour film lies between the superheated solid at $z' = 0$ and the evaporating liquid surface at $z' = h'(x', t')$. The liquid is cooled by a number of water-cooled pipes located at $z' = z'_L$. The interfacial mass flux is denoted by J' .

much larger and they stay attached to the heating surface instead of rising because of the reduced buoyancy force. In Space, the force of gravity becomes less important than the other forces such as surface tension, and film boiling is encountered more frequently. Thus, a more sophisticated and general theoretical approach is required to explain these differences and to predict how the change in system parameters affects the experiments. The small Bond number approximation presented in this paper is an important step in that direction.

Film boiling is characterized by two important parameters. The first is the *superheat* $\Delta T'_{SUP} = T'_S - T'_{SAT}$, the difference between the temperature of the solid and the saturation temperature. The second is the *subcooling* $\Delta T'_{SUB} = T'_{SAT} - T'_L$, the difference between the saturation temperature and the bulk temperature T'_L of the liquid. For low values of the superheat, the solid is either partially or completely wetted by the liquid. As the superheat increases, a critical value is reached where the vapour film completely covers the solid. This is called saturated film boiling if the subcooling is zero. Otherwise, it is known as subcooled film boiling. A general description of these and other pool boiling regimes can be found in Carey (1992).

In saturated film boiling, all of the heat conducted across the vapour film goes into evaporation. The average film thickness increases with time, and a flat liquid–vapour interface is Rayleigh–Taylor unstable because the vapour film lies beneath the heavier liquid. Vapour bubbles are released at the nodes of the instability, but as long as there is no significant liquid–solid contact, film boiling will continue.

In subcooled film boiling, some of the heat which would have gone into evaporation

is now removed by the cooler liquid. As a result, less vapour is produced when compared to saturated film boiling for the same superheat. In fact, if all of the heat conducted across the vapour film is removed by the cooler liquid, there is no energy left for evaporation, and the film is stationary. The particular film thickness which satisfies this condition is known as the equilibrium film thickness and can be determined by a simple heat-conduction balance. This unusual solution has been observed in the experiments of Abbassi & Winterton (1989) and Shoji & Kaneko (1986) for the largest subcooling that they consider. The existence of this solution was explained by Tanaka (1988), who showed that the stationary film is stable if its thickness is less than a certain critical value. Since the equilibrium thickness decreases as the subcooling is increased (with fixed superheat), the film is stable for sufficient subcooling.

The relationship between film boiling and the Rayleigh–Taylor instability was first mentioned by Chang (1959). Zuber (1959) postulated that the minimum solid-wall temperature required to sustain film boiling corresponds to the point where vapour is produced fast enough to compensate for the normal collapse rate of the film. Berenson (1961) used a lubrication approximation in the thin vapour film to arrive at a fairly accurate relationship between the observed heat flux and the surface temperature, but the shape of the liquid–vapour interface was fixed. Yiantsios & Higgins (1989) studied the Rayleigh–Taylor instability of thin viscous films beneath a heavier liquid but without evaporation. They derived a single, strongly-nonlinear equation which described the evolution of the film thickness. Burelbach, Bankoff & Davis (1988) used a similar approach to study evaporating liquid films on a horizontal solid plate, but there was no Rayleigh–Taylor instability because the liquid is beneath the vapour. A summary of these and other long-wave equations can be found in the review article by Oron, Davis & Bankoff (1997).

The present paper extends the analysis of Yiantsios & Higgins (1989) by including evaporative effects. The resulting evolution equation is used to study both saturated and subcooled film boiling, but particular emphasis is placed on the nonlinear, steady-state solutions of subcooled film boiling.

The film-boiling model is introduced in §2. A lubrication approximation is used in §3 to derive a strongly-nonlinear evolution equation satisfied by the film thickness. This equation is solved using a variety of methods. The linear stability of three different basic states is determined in §4. In particular, it is shown that the equilibrium film of subcooled film boiling is stable if the subcooling is large enough. A local bifurcation analysis is used in §5 to determine the solution structure near the neutrally-stable point. Numerical branch tracing is used in §6 to extend these solutions into the strongly-nonlinear regime. A number of initial-value problems are also solved in §6 in order to describe the early development of vapour bubbles and to verify the bifurcation results.

2. Formulation of the model

The current film-boiling model is shown in figure 1. The heating surface is located at $z' = 0$. Only two-dimensional disturbances are permitted for the moment, so the thickness of the vapour film is given by $z' = h'(x', t')$, where h' is a single-valued function of horizontal position x' and time t' . The single-valuedness assumption is no longer valid when vapour bubbles start to pinch off from the film. Thus, this model can only describe the early development of such bubbles.

The solid temperature T'_s is specified at a distance z'_s beneath the solid–vapour

interface in order to remove the thermal singularity which would be present as $h' \rightarrow 0$ if the temperature on the boiling surface and the temperature on the liquid–vapour interface were both fixed to different constants (cf. Oron, Bankoff & Davis 1996).

The method of achieving the subcooling varies from experiment to experiment, but typically, as in Abbassi & Winterton (1989), a number of water-cooled pipes are placed in the liquid at some distance z'_L above the heater surface. This is incorporated into the current model by setting the liquid temperature equal to T'_L at $z' = z'_L$. Since the liquid layer is heated from below and cooled from above, one might expect to see buoyancy-induced convection in the liquid. Indeed, natural convection is observed in the experiments of Abbassi & Winterton (1989) for their largest subcooling. However, the stable film is known to exist whether or not there is any convection. The effect of convection on the heat transfer is included in the current model by using an experimentally-determined heat-transfer coefficient which depends on the Rayleigh number in the liquid.

The liquid and vapour are both treated as incompressible, Newtonian fluids with constant material properties. It is assumed that the state of the vapour is completely determined by the horizontal and vertical velocity components u' and w' , pressure p' and temperature T' . The temperature of the solid is denoted by θ' . Since the liquid–vapour interface is a free surface, the film thickness h' is another unknown. Finally, J' is the mass flux across the liquid–vapour interface due to evaporation or condensation; $J' > 0$ for evaporation. The mass transfer is always assumed to be normal to the interface.

The boundary conditions on the solid surface at $z' = 0$ are no-slip, continuous temperature and continuous heat flux. On the free surface $z' = h'$, the boundary conditions represent a balance of mass, momentum and energy across an evaporating interface. These conditions were derived by Delhaye (1974) for an arbitrary surface but were written out in a useful component form by Burelbach *et al.* (1988).

It may seem inappropriate to treat the vapour as an incompressible fluid, but as long as the superheat is much less than the saturation temperature, this is a reasonable assumption. For example, if the vapour is treated as an ideal gas, the vapour density ρ is inversely proportional to the temperature. The temperature of the vapour changes from about T'_S near the solid surface to about T'_{SAT} near the liquid–vapour interface. The relative change in density is small as long as $\Delta T'_{SUP}/T'_{SAT} \ll 1$. In a typical experiment, $T'_{SAT} \approx 373$ K, $\Delta T'_{SUP} \approx 100$ K, and $\Delta T'_{SUP}/T'_{SAT} \approx 0.3$. Thus, for small to moderate superheat, incompressibility is reasonable, but for larger superheat, one may need to reconsider this assumption.

The term $-\rho g$ appears in the vertical momentum equation in the vapour in order to account for the gravitational body force, where g is the gravitational acceleration. Similarly, $-\rho_L g$ is the gravitational body force in the liquid, where ρ_L is the liquid density. The buoyancy force $\Delta \rho g$, where $\Delta \rho \equiv \rho_L - \rho$, is due to the jump in density across the liquid–vapour interface and is responsible for the Rayleigh–Taylor instability. If the roles of liquid and vapour were interchanged, there would no longer be any Rayleigh–Taylor instability because the heavier liquid would then lie beneath the vapour and buoyancy would actually be stabilizing.

A simple relationship between J' and T' is determined by considering the kinetic theory of an ideal gas (cf. Palmer 1976). If the departure from equilibrium is small, then it is appropriate to use this simple linear relationship,

$$K' J' = T' - T'_{SAT} \quad \text{at } z' = h', \quad (2.1)$$

where $K' = (8R_G^3 T'^5_{SAT} \pi^{-1} m^{-3})^{1/2} (\mathcal{L} p'_{SAT})^{-1}$ is called the disequilibrium number;

R_G is the ideal gas constant, m is the molar mass, \mathcal{L} is the latent heat per unit mass and p'_{SAT} is the saturation pressure corresponding to T'_{SAT} . The value of K' is typically much less than one, and the interfacial temperature remains close to equilibrium unless J' gets very large. This same equation was used by Burelbach *et al.* (1988) to study evaporating liquid films. For larger departures from equilibrium, Schrage (1953) derived a more general equation which reduces to (2.1) when linearized around the equilibrium point (cf. Panzarella 1998).

It is more convenient to work in terms of dimensionless variables. This is achieved by identifying a number of important dimensional scales, and the scaled variables are written without primes. There are several choices for the length scale, but the one chosen for the current paper is the average initial film thickness d . This length scale exists for both subcooled and saturated film boiling, unlike the equilibrium film thickness, for example, which only exists in the subcooled case. For saturated film boiling there are no steady solutions, and this is the most reasonable choice. For subcooled film boiling, one might wonder whether it is better to choose the initial film thickness or the equilibrium film thickness as the appropriate length scale. In order to avoid having to define different length scales for each case, the initial film thickness is chosen for both. The only apparent drawback is that certain results, such as the equilibrium solutions, are independent of d , and yet the solution, when written in terms of the dimensionless parameters, still seems to depend on it. However, in these cases, the dimensionless parameters, of course, always group together in such a way that the actual dependence on d cancels out. In the opinion of the authors, the generality of this choice outweighs any minor aesthetic difficulties that might arise. Furthermore, the initial film thickness is almost always chosen to be close to the equilibrium thickness when it exists, and so for practical purposes this choice is irrelevant. The numerical value of d in table 1 is on the order of the stable equilibrium film thickness observed by Abbassi & Winterton (1989).

Continuing with the non-dimensionalization, a typical pressure scale is the hydrostatic pressure difference $gd\Delta\rho$. The hydrostatic pressure is subtracted from p' before scaling by $gd\Delta\rho$ to obtain the dimensionless reduced pressure p in the vapour. The pressure in the liquid is scaled analogously. A typical velocity scale $gd^2\Delta\rho/\mu$ is found by balancing pressure and viscous forces in the vapour film, where μ is the dynamic vapour viscosity. The time scale $\mu/gd\Delta\rho$ is found by dividing the length scale by the velocity scale. The dimensionless temperatures measure relative deviation from the saturation temperature: $T = (T' - T'_{\text{SAT}})/T'_{\text{SAT}}$ and $\theta = (\theta' - T'_{\text{SAT}})/T'_{\text{SAT}}$ respectively. A mass-flux scale is found by balancing heat conduction across a film of constant thickness d with the energy required for evaporation, resulting in $k\Delta T'_{\text{SUP}}/d\mathcal{L}$, where k is the vapour thermal conductivity.

The properties of water at the boiling point are listed in table 1 along with those of a typical solid. Typical values of $\Delta T'_{\text{SUP}}$, $\Delta T'_{\text{SUB}}$, z'_S and z'_L are taken from the representative experiments of Abbassi & Winterton (1989).

3. The long-wave equation

A lubrication approximation in the vapour film results in a single, strongly-nonlinear evolution equation for the dimensionless film thickness h which retains the leading-order effects of evaporation, buoyancy and surface tension. A detailed derivation is not included in the current paper but can be found in Panzarella (1998). A review of other long-wave evolution equations and their applications is provided by Oron *et al.* (1997).

Properties of water:		Properties of copper:			
ρ	$0.6 \times 10^{-3} \text{ g cm}^{-3}$	ρ_S	8.9 g cm^{-3}		
ρ_L	0.96 g cm^{-3}	k_S	$4.0 \times 10^7 \text{ erg cm}^{-1} \text{ s}^{-1} \text{ K}^{-1}$		
μ	$1.26 \times 10^{-4} \text{ g cm}^{-1} \text{ s}^{-1}$	κ_S	$1.2 \text{ cm}^2 \text{ s}^{-1}$		
μ_L	$2.9 \times 10^{-3} \text{ g cm}^{-1} \text{ s}^{-1}$				
κ	$0.2 \text{ cm}^2 \text{ s}^{-1}$				
κ_L	$1.7 \times 10^{-3} \text{ cm}^2 \text{ s}^{-1}$				
k	$2.4 \times 10^3 \text{ erg cm}^{-1} \text{ s}^{-1} \text{ K}^{-1}$				
k_L	$6.8 \times 10^4 \text{ erg cm}^{-1} \text{ s}^{-1} \text{ K}^{-1}$				
σ	59 dyn cm^{-1}				
\mathcal{L}	$2.3 \times 10^{10} \text{ erg g}^{-1}$				
m	18 g mol^{-1}				
α_L	$7.5 \times 10^{-4} \text{ K}^{-1}$				
A'	10^{-13} erg				
Other parameters:		Dimensionless groups:			
p'_{SAT}	$101.3 \times 10^4 \text{ dyn cm}^{-2}$	A	5.63×10^{-10}	ΔT_{SUB}	4.02×10^{-2}
T'_{SAT}	373 K	B	1.60×10^{-3}	ΔT_{SUP}	2.68×10^{-1}
$\Delta T'_{\text{SUP}}$	100 K	E	8.68×10^{-3}	K	1.90×10^{-5}
$\Delta T'_{\text{SUB}}$	15 K	D_k	3.53×10^{-2}	z_L	10
d	0.01 cm	D_μ	4.34×10^{-2}	z_S	10
z'_L	0.1 cm	Γ_k	6.00×10^{-5}	H	1.12
z'_S	0.1 cm	R	2.87×10^3	Q	1.46
g	981 cm s^{-2}	G	35.6	A	6.19×10^{-4}
R_G	$8.31 \times 10^7 \text{ erg K}^{-1} \text{ mol}^{-1}$	N	1.58		
η	$6.8 \times 10^5 \text{ erg cm}^{-2} \text{ s}^{-1} \text{ K}^{-1}$				

TABLE 1. The material properties of water at the boiling point. A typical heater in the experiments is made of copper. Typical values of d , $\Delta T'_{\text{SUP}}$, $\Delta T'_{\text{SUB}}$, z'_S and z'_L are taken from the experiments of Abbassi & Winterton (1989).

The primary assumption used to derive the evolution equation is that the film thickness d is much less than the characteristic length of the instability λ' , i.e. $d \ll \lambda'$. This results in a small Bond number $B = d^2 \Delta \rho g / \sigma$, where σ is the surface tension. Since B measures the relative strength of buoyancy to surface tension, $B \ll 1$ means surface tension is much stronger than buoyancy. Since the effect of surface tension is stronger when the local film curvature is higher, short-wavelength disturbances are stabilized, and the remaining instability consists primarily of long wavelengths. From table 1, one can see that $B \ll 1$ for a typical film-boiling experiment, justifying the long-wave assumption. In terms of the dimensionless wavelength $\lambda = \lambda' / d$ or the dimensionless wavenumber $\beta = 2\pi / \lambda$, the long-wave assumption requires $\lambda \gg 1$ or $\beta \ll 1$.

The linear-stability analysis of the constant-thickness, isothermal film by Yiantsios & Higgins (1989) shows that the smallest dimensionless wavenumber that can be stabilized completely by surface tension is $B^{1/2}$ as $B \rightarrow 0$; a perturbation with wavenumber less than $B^{1/2}$ is unstable. The most unstable wavenumber (largest growth rate) is $(B/2)^{1/2}$, and its growth rate is $O(B)$ as $B \rightarrow 0$. For this reason, it is better to describe the instability in terms of the $O(1)$ coordinates $X = B^{1/2}x$ and $\tau = Bt$.

The long-wave assumption leads to a lubrication approximation in the vapour film. This means that the pressure in the film is independent of vertical position, $p_z = 0$,

and the horizontal pressure gradient is balanced by viscous forces, $B^{1/2}p_X = u_{zz}$ (the subscripts denote partial differentiation by the corresponding variable).

Since the dynamic viscosity of the liquid μ_L is normally much greater than that of the vapour (see table 1), the tangential component of velocity at the interface is nearly the same as the horizontal component of the bulk liquid velocity, which is assumed to be zero. To see this, consider the simplified form of the shear-stress boundary condition for a nearly-flat interface, i.e. $D_\mu u_z = u_z^L$, where $D_\mu = \mu/\mu_L$ is the viscosity ratio and u^L is the horizontal component of the liquid velocity. In the limit as $D_\mu \rightarrow 0$, $u_z^L \rightarrow 0$ and u^L has the same value at the interface as it does in the bulk liquid, namely $u^L = 0$ at $z = h$. Since the tangential component of velocity must be continuous across the interface, this also implies that $u = 0$ at $z = h$. This is the form of the boundary condition that is used in the present analysis. It is only strictly valid as long as $D_\mu u_z \ll 1$, and this may be violated if u_z gets too large. According to the lubrication approximation, $u_z = \frac{1}{2}B^{1/2}hp_X$ at $z = h$, so the boundary condition is valid as long as $|D_\mu B^{1/2}hp_X| \ll 1$. This is true as long as the pressure gradient p_X does not get too large. The forthcoming numerical results in §6.2 will show that $p_X \approx 0$ everywhere except at a few isolated points where the film thickness is minimum (in the gap region between bubbles). At those points, the vapour shear stress gets larger, but a comparison of the actual numerical values shows that this choice of boundary condition is still valid. For example, for the worst case in figure 12, the maximum value is $|D_\mu B^{1/2}hp_X| \approx 0.01 \ll 1$, and the boundary condition is likely to still be valid. If the pressure gradient became much larger, then the most general form of the shear-stress boundary condition would be required. This would lead to a non-trivial coupling between the long-wave equation and a solution of the Stokes equations in the liquid (cf. Yiantsios & Higgins 1989).

There is one finer point regarding the shear-stress boundary condition that should be mentioned. Although, the leading-order condition $u_z^L = 0$ at $z = h$ may still be valid, the assumption that the bulk liquid velocity is zero may not be. In fact, since the liquid is heated from below, natural convection is likely, and the bulk liquid velocity would then no longer be zero. The validity of the boundary condition $u = 0$ at $z = h$ would then be questionable. The condition $u = u^L$ is still appropriate, but a great deal of additional work would be required to determine the liquid velocity u^L at the interface (although it is certainly possible). This is not appropriate for the simple analysis striven for in the current paper, and for this reason, it is assumed that the boundary condition $u = 0$ at $z = h$ still holds even when natural convection is present. The effect of natural convection on the heat transfer is included in the model, however, by using an empirically-determined heat transfer coefficient as will be shown later.

The next boundary condition is the kinematic condition at the interface. The application of this boundary condition leads to the standard Reynolds equation for Poiseuille flow but modified to include evaporative effects,

$$h_\tau = \frac{E\Delta T_{\text{SUP}}}{B}J + \frac{1}{12}(h^3 p_X)_X, \quad (3.1)$$

where the evaporation number $E = k\mu T'_{\text{SAT}}/\rho\Delta\rho\mathcal{L}gd^3$ is the ratio of viscous to evaporative time scales, and $\Delta T_{\text{SUP}} = \Delta T'_{\text{SUP}}/T'_{\text{SAT}}$ is the dimensionless superheat. Note that in (3.1) the horizontal pressure gradient is multiplied by h^3 . This diminishes the effect of the pressure gradient as $h \rightarrow 0$.

Although not appropriate for the current analysis, it is interesting to note that if the boundary condition $u_z = 0$ (negligible liquid shear stress) had been used instead

of $u = 0$ at $z = h$, the fraction $\frac{1}{12}$ appearing in the above equation would be replaced by $\frac{1}{3}$. This shows that the particular choice of shear-stress boundary condition does not change the structure of the dynamics, but it does tend to modify the growth rate of the instability. In reality, the actual solution probably lies somewhere between these two extremes.

The dimensionless reduced pressure p , which is independent of z , is determined from the long-wave form of the normal-stress boundary condition at the free surface,

$$p = -h - h_{XX} \quad \text{at } z = h. \quad (3.2)$$

The first and second terms respectively account for buoyancy and surface tension.

The dimensionless mass flux J is determined by solving one-dimensional, steady heat equations in the vapour and solid,

$$T_{zz} = \theta_{zz} = 0. \quad (3.3)$$

The superheat is prescribed at $z = -z_S = -z'_S/d$,

$$\theta = \Delta T_{\text{SUP}} \quad \text{at } z = -z_S, \quad (3.4)$$

and the temperature and heat flux are continuous at the solid–vapour interface,

$$\theta = T \quad \text{at } z = 0, \quad (3.5)$$

$$\theta_z = \Gamma_k T_z \quad \text{at } z = 0, \quad (3.6)$$

where $\Gamma_k = k/k_S$ is the ratio of vapour to solid thermal conductivity.

An energy balance across the free surface results in

$$\Delta T_{\text{SUP}} J = -\frac{N}{D_k z_L} (T + \Delta T_{\text{SUP}}) - T_z \quad \text{at } z = h, \quad (3.7)$$

where $D_k = k/k_L$ is the ratio of vapour to liquid thermal conductivities and $N = \eta z'_L/k_L$ is the Nusselt number corresponding to the dimensional heat-transfer coefficient η . This is combined with the dimensionless form of (2.1),

$$K \Delta T_{\text{SUP}} J = T \quad \text{at } z = h, \quad (3.8)$$

to eliminate J in (3.7); $K = kK'/d\mathcal{L}$ is the dimensionless disequilibrium number. This is the only remaining boundary condition needed to solve for the temperatures. Once the temperatures are known, J is computed from (3.7).

If there were no motion in the liquid, then the heat transfer would be due solely to steady heat conduction in the liquid and $N = 1$ (assuming $d/z'_L \ll 1$ so that variations in the film thickness do not significantly affect the liquid heat flux). Temperature-induced buoyancy effects may lead to convection in the liquid which would enhance the heat transfer on the liquid side of the interface. In general, this is represented by a relationship between N and the Rayleigh number $R = \rho_L g \alpha_L \Delta T'_{\text{SUB}} z_L'^3 / \mu_L \kappa_L$ in the liquid, which measures the relative importance of buoyancy to viscous effects; α_L is the coefficient of thermal expansion in the liquid and κ_L is the thermal diffusivity of the liquid. For natural convection between two horizontal plates separated by a distance z'_L , an experimental correlation is determined by Hollands, Raithby & Konicek (1975). Since there is no rigid surface in the liquid, this relationship is modified to use the critical Rayleigh number valid for rigid-free boundaries. In addition, only the first mode of instability is considered. With these modifications, the empirical relationship

becomes

$$N = \begin{cases} 1, & R < 1101 \\ 1 + 1.44 \left(1 - \frac{1101}{R}\right), & R > 1101. \end{cases} \quad (3.9)$$

When $R < 1101$, there is no motion in the liquid and the heat transfer is due to steady heat conduction only. For higher values of R , the heat transfer is enhanced by natural convection. The above correlation also assumes that the liquid temperature profile has had sufficient time to reach steady state. This may not always be the case, and a more general treatment would permit N to be a function of time as well as R , i.e. $N = N(R, \tau)$.

Only the steady form of N is required for the present analysis since the threefold focus of this paper is to determine the equilibrium solutions of subcooled film boiling, the slow dynamics near equilibrium and the much faster dynamics of saturated film boiling. In the first case, the equilibrium solutions obviously only depend on the steady form of N . In the second case, the time scale of the film dynamics can be made arbitrarily large, by choosing the initial state of the system to be close enough to equilibrium, in order to give the liquid temperature enough time to reach steady state before the interface deforms appreciably. In the saturated case, there is no heat loss on the liquid side of the interface since the subcooling is zero, and so the particular value of N does not really matter anyway. The only situation where the transient nature of N is important would be the approach to equilibrium in strongly-subcooled film boiling if the initial temperature gradient on the liquid side of the interface were zero. This is a special case because the system would start out behaving like saturated film boiling (rapid instability), but as the liquid near the interface cools, the amount of evaporation would decrease, and the system would eventually behave like subcooled film boiling near equilibrium. The open question here is whether or not the increasing liquid heat flux would have sufficient time to suppress the instability before the film deformation leads to vapour-bubble detachment. Since this is a much more complicated question that deserves a separate detailed analysis, this case will not be examined in the present paper. Instead, it will always be assumed that the liquid near the interface has had sufficient time to reach steady state before the onset of the instability. This restricts the choice of initial conditions somewhat, but there is still a considerable amount to be learned by doing so.

The solution of this steady-state thermal problem yields a simple relationship between J and h ,

$$J = \frac{BQ}{E\Delta T_{\text{SUP}}} \frac{1 - h/H}{h + A}, \quad (3.10)$$

where

$$H = \frac{\Delta T_{\text{SUP}}}{\Delta T_{\text{SUB}}} \frac{D_k z_L}{N} - \Gamma_k z_S \quad (3.11)$$

is the dimensionless equilibrium thickness (the ratio of the dimensional equilibrium thickness to the initial film thickness d),

$$Q = \frac{E(\Delta T_{\text{SUP}} D_k z_L - \Delta T_{\text{SUB}} N \Gamma_k z_S)}{B(D_k z_L + KN)} \quad (3.12)$$

measures the heating of the solid, and

$$A = \frac{D_k \Gamma_k z_L z_S + K D_k z_L + KN \Gamma_k z_S}{D_k z_L + KN} \quad (3.13)$$

accounts for the non-equilibrium evaporation condition and the thermal resistance of the solid plate. Typical values of H , Q and A are also listed in table 1.

The mass flux J increases as h decreases and is bounded as $h \rightarrow 0$ as long as $A \neq 0$, which is the case if either the solid has a finite thermal conductivity or if one uses a non-equilibrium evaporation condition at the interface (cf. Oron *et al.* 1996).

Substituting J and p into (3.1) results in a single, strongly-nonlinear evolution equation satisfied by the film thickness h ,

$$h_\tau = Q \frac{1 - h/H}{h + A} - \frac{1}{12} [h^3(h + h_{XX})_X]_X. \quad (3.14)$$

The first term on the right-hand side of (3.14) is due to evaporative mass loss, and the second and third terms include the effects of buoyancy and surface tension, respectively. This equation is almost identical to the one derived by Burelbach *et al.* (1988) except for the form of the mass-loss term. Q is now positive because the direction of evaporation is reversed from that of Burelbach *et al.* (1988), and the buoyancy term changes sign because the roles of liquid and vapour are interchanged. This makes evaporation stabilizing for film boiling, whereas it is destabilizing for liquid films. Similarly, although buoyancy is stabilizing for a liquid film, it is the driving mechanism behind the Rayleigh–Taylor instability of film boiling. The surface-tension term remains the same because a negative film curvature increases the local film pressure regardless of whether the film is liquid or vapour. Thus, even though this equation resembles those used previously to study liquid films, the nature of the solutions is quite different.

The derivation of this evolution equation places no restriction on the value of h other than it not become extremely large or small (by an order of magnitude) and as long as $h_x \ll 1$ ($h_x \ll B^{-1/2}$). Otherwise, neglected terms may no longer be negligible. This is why (3.14) is called a *strongly-nonlinear* evolution equation, as opposed to a weakly-nonlinear equation which would only be valid if h were arbitrarily close to some basic-state solution. The small-slope assumption always breaks down as vapour bubbles pinch off from the film because the slope becomes infinite. Thus, the evolution equation is only able to describe the early development of such vapour bubbles. A boundary-element method is used in Panzarella (1998) to extend these solutions all the way up to the point where the bubble pinches off from the film since it removes the restriction on the shape of the liquid–vapour interface.

3.1. Subcooled film boiling

In subcooled film boiling, both the subcooling ΔT_{SUB} and the superheat ΔT_{SUP} are non-zero. There is a simple steady-state solution $h = H$ with a dimensional film thickness

$$d_E = Hd = \frac{\Delta T_{\text{SUP}}}{\Delta T_{\text{SUB}}} \frac{D_k z'_L}{N} - \Gamma_k z'_S. \quad (3.15)$$

This is the particular film thickness which exactly balances the heat conducted across the film with the heat loss due to liquid subcooling. The special case $H = 1$ corresponds to the situation where the average initial film thickness d is equal to the equilibrium thickness d_E . It is easy to show that the arbitrary H equation is equivalent to an $H = 1$ equation (except for the initial conditions) by the simple transformation: $h = H\bar{h}$, $Q = H^5\bar{Q}$, $A = H\bar{A}$ and $\tau = H^{-3}\bar{\tau}$. Substituting this into (3.14) yields the

following equation in terms of the new variables:

$$\bar{h}_\tau = \bar{Q} \frac{1 - \bar{h}}{\bar{h} + \bar{A}} - \frac{1}{12} [\bar{h}^3 (\bar{h} + \bar{h}_{XX})_X]_X. \quad (3.16)$$

Note that this equation has exactly the same form as (3.14) except that now $H = 1$. This is just another way of showing that one could have just as easily chosen the length scale to be the equilibrium thickness d_E , when it exists. This would have made $H = 1$, but then the other parameters would have depended on the superheat and subcooling through the parameter d_E . This is undesirable, however, because it is much better to choose a scaling such that the superheat and subcooling are independently adjustable parameters since this has a more direct physical interpretation in the experiments.

The only thing preventing an arbitrary H solution from being identical to an $H = 1$ solution is the initial conditions. If the initial condition for h is $h = h_0(X)$ at $\tau = 0$, then the initial condition in terms of \bar{h} is $\bar{h} = H^{-1}h_0(X)$. For those situations in which the initial conditions are not important, e.g. linear stability and bifurcation analyses, results from the $H = 1$ solution can be immediately transformed into arbitrary H results. An example of this will be given in §4.3.

3.2. Saturated film boiling

The saturated case is obtained when the subcooling is zero ($\Delta T_{\text{SUB}} = 0$). If the superheat is fixed, then $H \rightarrow \infty$ and the evolution equation becomes

$$h_\tau = \frac{Q}{h + A} - \frac{1}{12} [h^3 (h + h_{XX})_X]_X. \quad (3.17)$$

There are no stationary solutions in saturated film boiling since all the heat conducted across the film goes into evaporation. The average film thickness always increases, and an equilibrium thickness does not exist. Since the subcooling is zero, Q increases linearly with increasing superheat,

$$Q = \frac{E \Delta T_{\text{SUP}}}{B}. \quad (3.18)$$

3.3. Isothermal film

When the superheat and subcooling are both zero ($Q = 0$), the resulting evolution equation is

$$h_\tau = -\frac{1}{12} [h^3 (h + h_{XX})_X]_X. \quad (3.19)$$

This same equation was used by Yiantsios & Higgins (1989) to study the Rayleigh–Taylor instability of thin viscous films beneath a heavier liquid. Any constant h satisfies this equation but is always unstable due to buoyancy forces. Surface tension stabilizes the short-wavelength disturbances, but the long-wavelength disturbances will eventually dominate. The instability will either lead to the release of a vapour bubble, or the film will approach a particular steady-state solution consisting of a sinusoidal bubble attached to the solid surrounded by a zero-thickness film. It takes an infinite amount of time to reach this steady state, however, because the minimum film thickness decays like $\tau^{-1/2}$ (cf. Hammond 1983).

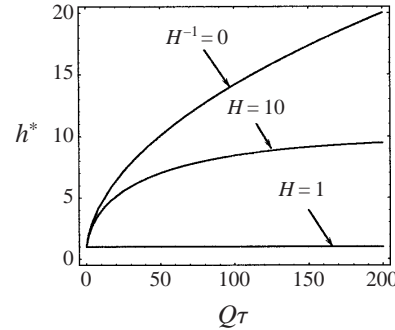


FIGURE 2. The basic-state film thickness h^* given by (4.1) when $A = 0$: $H = 1$, steady subcooled film boiling; $H = 10$, time-dependent subcooled film boiling; $H^{-1} = 0$, time-dependent saturated film boiling.

4. Linear stability of basic states

The spatially-uniform solutions of (3.14) for arbitrary H satisfy

$$\frac{dh^*}{d\tau} = Q \frac{1 - h^*/H}{h^* + A} \quad \text{with } h^*(0) = 1. \quad (4.1)$$

The film thickness remains constant when $h^* = H$, decreases if $h^* > H$, and increases when $h^* < H$. However, since the solution must always start at $h^* = 1$ (since the length scale d is the average initial film thickness), there are three different cases depending on the value of H , as shown in figure 2. When $H = 1$, the initial film thickness is equal to the equilibrium film thickness, and the solution is stationary for all times. When $H \neq 1$ but still finite, the solution will evolve from the initial value $h^* = 1$ to the final value $h^* = H$ according to (4.1). When $H^{-1} = 0$, there are no steady solutions, and the film thickness increases without bound. The first two cases arise in subcooled film boiling while the last occurs only in saturated film boiling. Note that any solution of (4.1) evolves on the evaporative time scale $Q\tau$. The film growth is slower as Q gets smaller because the rate of evaporation is reduced. When $Q = 0$, there is no preferred film thickness, but the only solution which satisfies the initial condition is $h^* = 1$.

The stability of any basic state h^* is determined by substituting $h = h^*(\tau) + a \exp(s(\beta, \tau)\tau + i\beta X)$ into (3.14) and solving for the leading-order growth rate when $|a| \ll 1$,

$$s(\beta, \tau) = \frac{1}{\tau} \int_0^\tau \left[\frac{1}{12} \beta^2 (1 - \beta^2) h^{*3} - \frac{Q(H^{-1}A + 1)}{(h^* + A)^2} \right] d\tau. \quad (4.2)$$

This depends on the wavenumber β and is time-dependent if the basic state is time-dependent. The basic state is unstable if this growth rate remains positive as $\tau \rightarrow \infty$.

The wavenumber of the perturbation must be restricted in order to be consistent with the long-wave assumption. Since $\beta X = \beta B^{1/2} x$, this requires $\beta B^{1/2} \ll 1$ or $\beta \ll B^{-1/2}$ as $B \rightarrow 0$. The subsequent results show that the unstable wavenumbers lie in the range $0 < \beta < 1$, and this is consistent with the long-wave assumption.

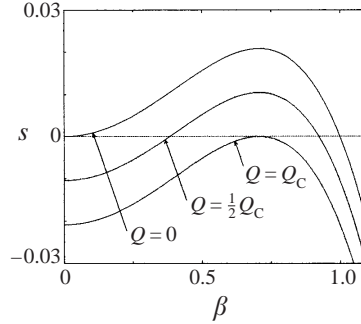


FIGURE 3. Growth rate s vs. wavenumber β for linear stability of steady subcooled basic state when $H = 1$ and $A = 0$. The basic state is stable when $Q > Q_C$.

4.1. Case $H = 1$

For the special case $H = 1$, the average initial film thickness is equal to the equilibrium thickness so that the basic state is $h^*(\tau) = 1$, and the constant linear growth rate is

$$s(\beta) = \frac{1}{12}\beta^2(1 - \beta^2) - \frac{Q}{1 + A}. \quad (4.3)$$

The maximum growth rate occurs at the most unstable wavenumber $\beta_{\text{MAX}} = 1/\sqrt{2}$. Increasing Q decreases each growth rate by the same constant amount. There is a critical value,

$$Q_C = \frac{1 + A}{48}, \quad (4.4)$$

greater than which all the growth rates are negative and the basic state is linearly stable. A plot of the growth rate versus wavenumber for three different values of Q is shown in figure 3 when $A = 0$. The basic state is stable when $Q > Q_C$.

4.2. Case $H^{-1} = 0$

Next, consider the time-dependent basic state of saturated film boiling when $A = 0$,

$$h^*(\tau) = (2Q\tau + 1)^{1/2}. \quad (4.5)$$

The corresponding time-dependent growth rate is

$$s(\beta, \tau) = \frac{1}{30}\beta^2(1 - \beta^2) \left[\frac{(2Q\tau + 1)^{5/2} - 1}{2Q\tau} \right] - \frac{Q \ln(2Q\tau + 1)}{2Q\tau}, \quad (4.6)$$

and the initial behaviour is found by expanding in powers of $Q\tau$,

$$s(\beta, \tau) \sim \frac{1}{12}\beta^2(1 - \beta^2) \left(1 + \frac{3}{2}Q\tau \right) - Q + Q^2\tau, \quad |Q\tau| \ll 1. \quad (4.7)$$

If $Q > Q_C$, all the growth rates are initially negative, and there is an early period of stabilization. However, the long-time asymptotic behaviour,

$$s(\beta, \tau) \sim \frac{\sqrt{2}}{15}\beta^2(1 - \beta^2)(Q\tau)^{3/2}, \quad |Q\tau| \gg 1, \quad (4.8)$$

shows that the growth rate for all wavenumbers less than unity will eventually become positive. Thus, the saturated basic state is always unstable even though there might be an early period of stabilization. Figure 4(a) shows the growth rate vs. wavenumber given by (4.6) for three different times when $Q = 2Q_C$. Since $Q > Q_C$,

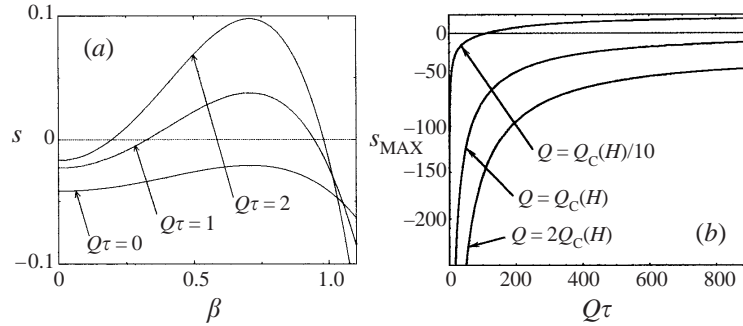


FIGURE 4. Time-dependent growth rates $s(\beta, \tau)$ for linear stability of time-dependent basic states when $\Lambda = 0$: (a) saturated film boiling ($H^{-1} = 0$) with $Q = 2Q_C$; (b) maximum growth rate $s_{\text{MAX}} = s(\beta_{\text{MAX}}, \tau)$ for subcooled film boiling when $H = 10$.

all perturbations are initially damped, but long-wavelength instabilities eventually dominate. Since stabilization is observed only as long as $\tau \ll Q^{-1}$, increasing Q will provide the initial stabilization but at the cost of decreasing the period of time over which it can be observed.

4.3. Case $1 < H < \infty$

There is a time-dependent basic state in subcooled film boiling when the initial film thickness is less than the equilibrium thickness ($1 < H < \infty$), but the solution can only be obtained in implicit form,

$$h^*(\tau) = H + (1 - H) \exp\left(\frac{1 - h^* - QH^{-1}\tau}{H + \Lambda}\right). \quad (4.9)$$

The corresponding growth rate is determined by numerically integrating (4.2).

When $H \gg 1$, the film will initially behave like saturated film boiling, but as time increases the thickness approaches the equilibrium value $h^* = H$, and the growth rate approaches the constant

$$s(\beta) = \frac{1}{12}H^3\beta^2(1 - \beta^2) - \frac{Q}{H(H + \Lambda)}. \quad (4.10)$$

If this is negative for every wavenumber, then the basic state is stable. This is achieved by selecting Q larger than the critical value

$$Q_C(H) = \frac{H^4(H + \Lambda)}{48}, \quad (4.11)$$

which depends on H but reduces to (4.4) when $H = 1$. The growth rate of the most-unstable wavenumber is graphed in figure 4(b) for a few different values of Q and is always negative when $Q > Q_C(H)$. Note that (4.11) can be obtained from (4.4) by the substitutions $Q \rightarrow Q/H^5$ and $\Lambda \rightarrow \Lambda/H$ as mentioned in § 3.1.

4.4. Summary of linear-stability results

When $H = 1$, the steady basic state $h^* = 1$ is stable if $Q > Q_C$. The time-dependent basic state of saturated film boiling ($H^{-1} = 0$) is always unstable, but there may be an initial period of stabilization if Q is large enough. Finally, the time-dependent approach to the subcooled equilibrium solution ($1 < H < \infty$) is stable if Q is large enough to stabilize the final equilibrium solution $h^* = H$.

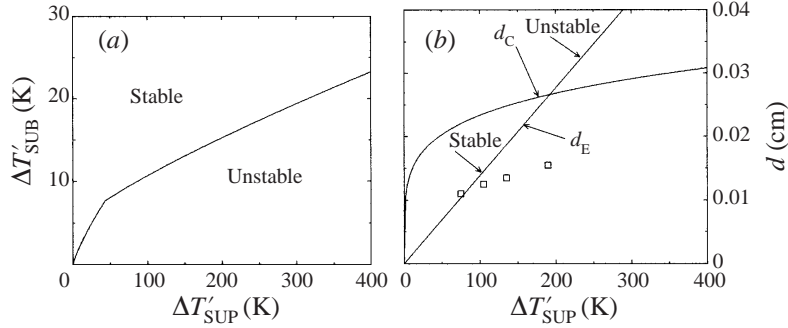


FIGURE 5. (a) The neutral-stability curve defined by (4.14) and (4.15) in terms of the dimensional superheat $\Delta T'_{\text{SUP}}$ and subcooling $\Delta T'_{\text{SUB}}$ for the properties of water in table 1. (b) Neutral-stability curve in terms of the dimensional film thickness d . A vapour film with equilibrium film thickness d_E , given by (3.15), is stable if $d_E < d_C$, where d_C is the critical film thickness given by (4.16). The subcooling is fixed to $\Delta T'_{\text{SUB}} = 15$ K. The other material properties are taken from table 1. The square data points \square are the experimental measurements of d_E for the stable film as determined by Abbassi & Winterton (1989). No stable film is observed in the experiments when $\Delta T'_{\text{SUP}} > 200$ K.

The steady basic state is neutrally stable when $Q = Q_C$. Since Q has no direct physical interpretation, it is more useful to have a relationship between the superheat and the subcooling because these are two of the most easily-controlled parameters in the experiments. If the superheat and subcooling are varied independently of one another, then H will change as well. Thus, the form of the critical value $Q_C(H)$ which depends on H is required. First, note that Q can be written as

$$Q = \frac{E\Delta T_{\text{SUB}}NH}{B(D_k z_L + KN)}. \quad (4.12)$$

Thus, the stability condition $Q = Q_C(H)$ becomes

$$\frac{E\Delta T_{\text{SUB}}NH}{B(D_k z_L + KN)} = \frac{H^4(H + A)}{48}. \quad (4.13)$$

The only parameters in the previous equation which depend on the superheat or the subcooling are H and N . It is also possible to show, with the help of a little algebra, that (4.13) is independent of the arbitrary initial film thickness d as it should be. By using the material properties in table 1 and neglecting the very small terms involving A and K , the numerical form of (4.13) becomes

$$N\Delta T_{\text{SUB}} = 0.11605\Delta T_{\text{SUP}}^{4/5}, \quad (4.14)$$

and N depends on the subcooling according to the following numerical relationship:

$$N = \begin{cases} 1, & \Delta T'_{\text{SUB}} < 7.68 \text{ K} \\ 2.44 - \frac{11.08 \text{ K}}{\Delta T'_{\text{SUB}}}, & \Delta T'_{\text{SUB}} > 7.68 \text{ K}. \end{cases} \quad (4.15)$$

These last two equations are used to construct the neutral-stability curve shown in figure 5(a). This shows that for each particular value of the superheat, the film is stable for sufficient subcooling. Likewise, if the subcooling is fixed, the film is stable if the superheat is small enough. The sudden change in slope at $\Delta T'_{\text{SUP}} = 43.0$ K corresponds to the onset of natural convection at $\Delta T'_{\text{SUB}} = 7.68$ K. For a larger superheat, convection enhances the liquid heat transfer, and less subcooling is required

to remove the same amount of heat than if there were no convection. For example, if the subcooling is fixed to $\Delta T'_{\text{SUB}} = 15$ K, the basic state is stable if $\Delta T'_{\text{SUP}} < 192.72$ K. If there were no convection, then a subcooling of at least $\Delta T'_{\text{SUB}} = 25.5$ K would be required to stabilize the film for the same superheat.

Since the dimensional film thickness is related to the superheat and subcooling by (3.15), it is possible to restate the neutral-stability condition in terms of the film thickness. For example, substituting the critical value of $N\Delta T_{\text{SUB}}$ given by (4.14) into (3.15) yields the critical value of the dimensional film thickness,

$$d_C = 0.030418 \text{ cm } \Delta T'_{\text{SUP}}{}^{1/5}, \quad (4.16)$$

less than which the film is stable. Depending on the actual value of the subcooling, the equilibrium thickness d_E may be less than or greater than this critical value. If $d_E < d_C$, then the film is stable. Otherwise, it is unstable. For example, if the subcooling is fixed to $\Delta T'_{\text{SUB}} = 15$ K, then d_E increases linearly with increasing superheat as shown in figure 5(b). Also shown in the figure is the critical thickness d_C . The two curves intersect when $\Delta T'_{\text{SUP}} = 192.72$ K. Thus, the basic state is stable when $\Delta T'_{\text{SUP}} < 192.72$ K and unstable when $\Delta T'_{\text{SUP}} > 192.72$ K. This is reasonably consistent with the experimental measurements of d_E by Abbassi & Winterton (1989) which are also shown in figure 5(b) as the square data points. They only observed the stable vapour film when $\Delta T'_{\text{SUP}} < 200$ K, coinciding with the predicted intersection of the two curves. However, experimental data for strongly-subcooled film boiling are scarce, and more precisely-controlled experiments are necessary before drawing further conclusions.

In order to understand how a thin vapour film can be stabilized by evaporation, consider a small perturbation of the equilibrium thickness $h' = d_E$. The resulting film thickness will be less than d_E in some places and greater than d_E in others. Liquid closer to the solid wall receives a greater heat flux, and the extra associated energy quickly evaporates the incoming liquid. Since the rate of evaporation increases as the equilibrium thickness decreases as shown in (3.10), the liquid will evaporate faster for the same perturbation if the equilibrium film is thinner. For a sufficiently thin film, the liquid evaporates fast enough to compensate for the growth rate of the instability in the absence of evaporative effects. This moves the liquid away from the wall and back towards equilibrium. Likewise, liquid further from the wall receives less heat from the solid, the interfacial vapour condenses and the liquid moves back towards equilibrium. Thus, the basic state is stable if the equilibrium film is thin enough. Since the equilibrium thickness decreases as the subcooling increases (with fixed superheat) as shown by (3.15), the basic state is stable for sufficient subcooling.

5. Local bifurcation analysis

For simplicity, assume that the average initial film thickness d is equal to the equilibrium thickness d_E by choosing $H = 1$. The results for arbitrary H can be obtained from the $H = 1$ results by the transformation described in §3.1.

The steady basic state $h = 1$ is unstable when $Q < Q_C$, but when $\delta = 1 - Q/Q_C$ is close to zero, there is a supercritical bifurcation to a branch of spatially-periodic equilibrium solutions at $Q = Q_C$. In order to see this, consider periodic solutions of (3.14) on the interval $-\lambda/2 < X < \lambda/2$,

$$h(X, \tau) = 1 + \sum_{n=-\infty}^{\infty} a_n(\tau) e^{in\beta X}, \quad (5.1)$$

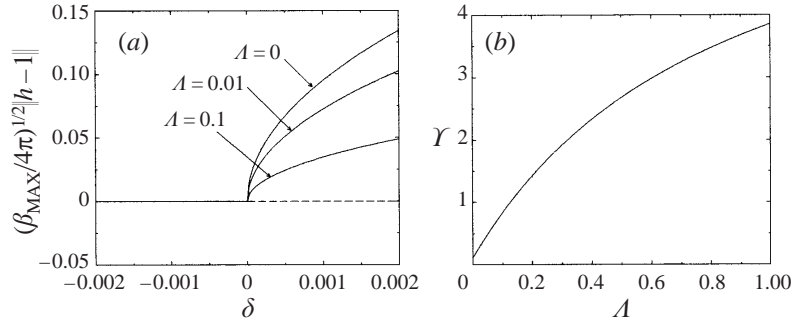


FIGURE 6. Equilibrium solutions near the bifurcation point $\delta = 0$ for subcooled film boiling on a periodic interval when $\beta = \beta_{\text{MAX}}$ and $H = 1$. (a) Bifurcation diagram determined from the Landau equation (5.7) in terms of the solution norm (5.10): —, stable; ---, unstable. (b) Landau coefficient γ as it depends on A .

where $\beta = 2\pi/\lambda$ is the wavenumber associated with the spatial period λ and a_n is the time-dependent amplitude of the n th Fourier mode. In order to measure departure from the basic state, a solution norm is defined by

$$\|h - 1\|^2 \equiv \int_{-\lambda/2}^{\lambda/2} (h - 1)^2 dX. \quad (5.2)$$

Equation (5.1) is substituted into (3.14) resulting in a system of equations satisfied by the complex Fourier amplitudes,

$$\dot{a}_n = s_n a_n + \sum_{j=-\infty}^{\infty} N_{2,n,j} a_j a_{n-j} + \sum_{j=-\infty}^{\infty} \sum_{k=-\infty}^{\infty} N_{3,n,j,k} a_j a_k a_{n-j-k} + O(a^4), \quad (5.3)$$

where the

$$s_n = \frac{\beta_{\text{MAX}}^4}{12} \left[\delta - \left(n^2 \frac{\beta^2}{\beta_{\text{MAX}}^2} - 1 \right)^2 \right] \quad (5.4)$$

are the discrete linear growth rates, and

$$N_{2,n,j} = \frac{1}{4} \beta^2 n(n-j) [1 - (n-j)^2 \beta^2] + \frac{\beta_{\text{MAX}}^4 (1-\delta)}{12(1+A)}, \quad (5.5)$$

$$N_{3,n,j,k} = \frac{1}{4} \beta^2 n(n-j-k) [1 - (n-j-k)^2 \beta^2] - \frac{\beta_{\text{MAX}}^4 (1-\delta)}{12(1+A)^2} \quad (5.6)$$

are the constant coefficients of the quadratic and cubic nonlinear terms, respectively (cf. Panzarella 1998).

The largest value of s_n is obtained when $\beta_{\text{MAX}}/\beta = n$, when λ is an integer multiple of the most unstable wavelength. When $\beta = \beta_{\text{MAX}}$, all of the growth rates are negative except for s_1 , which is positive if $\delta > 0$ and negative if $\delta < 0$. The basic state is neutrally stable when $\delta = 0$, and the local solution structure is determined by carefully scaling the Fourier amplitudes: $a_0 = O(\delta)$, $a_n = O(\delta^{n/2})$ for $n \geq 1$, and $\tau = O(\delta^{-1})$. The leading-order solution in δ yields a Landau equation for the most unstable mode a_1 ,

$$\dot{a}_1 = \frac{\beta_{\text{MAX}}^4}{12} a_1 (\delta - \gamma |a_1|^2), \quad (5.7)$$

where

$$\gamma = \frac{1 + 75A + 63A^2}{9(1 + A)^2} \quad (5.8)$$

is the Landau coefficient. γ is positive and so the bifurcation is always supercritical.

When $\delta > 0$, the film thickness on the bifurcated solution branch is given by

$$h = 1 + 2 \left(\frac{\delta}{\gamma} \right)^{1/2} \cos(\beta_{\text{MAX}} X) + O(\delta). \quad (5.9)$$

The corresponding solution norm,

$$\|h - 1\| = \left(\frac{4\pi}{\gamma\beta_{\text{MAX}}} \right)^{1/2} \delta^{1/2}, \quad (5.10)$$

is graphed in figure 6(a) for three different values of A . Thus, as δ increases past zero, the basic state loses stability to a new branch of spatially-periodic equilibrium solutions.

Since γ increases as A increases, as shown in figure 6(b), the solution norm decreases with increasing A . If interfacial equilibrium is assumed by choosing $K = 0$, then A reduces to $A = \Gamma_k z_S$. This shows that A is simply proportional to the thickness of the substrate and inversely proportional to its thermal conductivity. Thus, for a fixed value of δ the amplitude of the bifurcated solution decreases as the thermal conductivity of the solid decreases or as the plate thickness increases.

6. Numerical solutions of the long-wave equation

Additional results are obtained by numerically solving the long-wave equation, but only periodic solutions with the most-unstable wavelength are considered here. The results of Yiantsios & Higgins (1989) indicate for the isothermal problem that the effect of changing the period of the solution is minimal. Thus, the evolution equation is solved on the most-unstable interval $-\sqrt{2}\pi < X < \sqrt{2}\pi$ with periodic boundary conditions. A pseudo-spectral method is employed to evaluate the spatial derivatives at a discrete number of grid points, and the time-dependent behaviour is determined by solving the resulting nonlinear system of ordinary differential equations using the `lsode` subroutine (cf. Petzold 1983). The accuracy of this method is monitored by ensuring that the initial growth rate of the instability agrees with that predicted by linear stability and that the film volume in the isothermal case remains constant.

The equilibrium solutions are found by using the numerical bifurcation and branch-tracing code AUTO developed by Doedel (1981). The Landau equation (5.7) provides a starting point for AUTO, which then follows the solution branch into the strongly-nonlinear regime. All of the bifurcation results presented here are for the case $H = 1$, but this is not a restriction as discussed in §3.1. The bifurcation results do not depend on the initial conditions.

Two types of equilibrium solutions are found using AUTO. The first are steady-state solutions satisfying $h_\tau = 0$, and the second are travelling waves satisfying $h_\tau = \pm ch_X$ with an *a priori* unknown wave speed c ; this is an additional degree of freedom that needs to be determined along with the shape of the film profile. A phase condition like the one described by Aston, Spence & Wu (1992) is used to isolate points on the group orbit of solutions resulting from the translational and reflectional symmetry of this problem (due to the periodic boundary conditions).

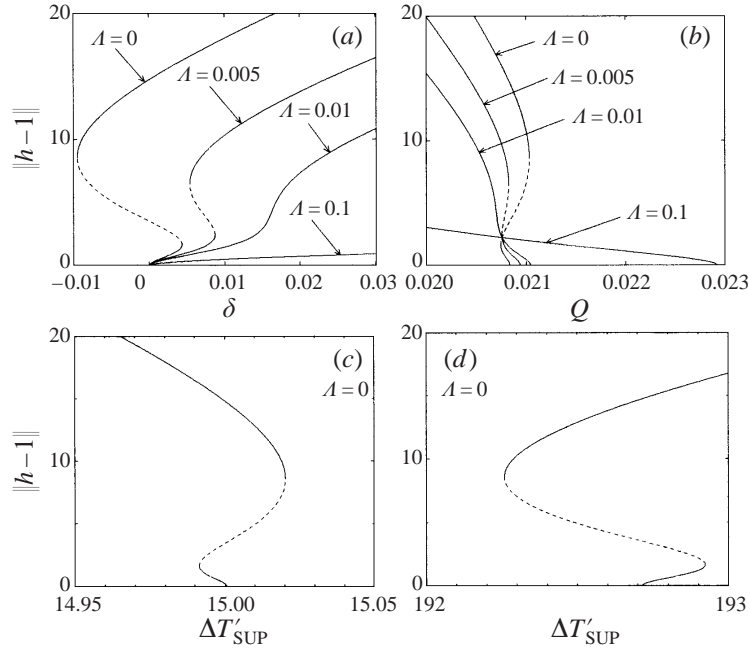


FIGURE 7. Bifurcation diagram for subcooled film boiling showing the influence of the solid thermal resistance A when $H = 1$: —, stable; ---, unstable. The bifurcation parameter is (a) δ ; (b) Q ; (c) $\Delta T'_{\text{SUB}}$ when $\Delta T'_{\text{SUP}} = 192.72$ K; (d) $\Delta T'_{\text{SUP}}$ when $\Delta T'_{\text{SUB}} = 15$ K. The required material properties are taken from table 1. The two turning points are at $\delta = 0.00434$ and $\delta = -0.00949$ when $A = 0$. There are 256 spectral modes.

6.1. Steady states and travelling waves

The non-trivial branch of steady solutions originating from the bifurcation point at $\delta = 0$ is continued into the strongly-nonlinear regime for several different values of A . The most compact form of the resulting bifurcation diagram is shown in figure 7(a). The same data are shown in figure 7(b) but with Q as the bifurcation parameter. This shows how the primary bifurcation point Q_C increases as A increases.

When $A = 0$, there is a continuous transition as δ is increased past $\delta = 0$, from the uniform basic state to the variable film thickness predicted by the Landau equation (5.7), but as δ is increased past the first turning point at $\delta = 0.00434$, there is a sudden transition to a larger-amplitude solution on the upper branch. Once on the upper branch, there is another transition back down to the basic state as δ is decreased below the second turning point at $\delta = -0.00949$. This is typical of hysteretic behaviour.

From a practical viewpoint, it is more interesting to know how the equilibrium solutions depend directly on the superheat and the subcooling since these two parameters are easily controlled in experiments. This is done by replotting the bifurcation diagram in terms of the superheat and subcooling by substituting (4.11) and (4.12) into the definition of δ . By using the material properties in table 1 and neglecting the small terms involving Γ_k , A and K , the numerical relationship between δ , $\Delta T'_{\text{SUP}}$ and $\Delta T'_{\text{SUB}}$ is

$$\delta = 1 - 4.7508 \times 10^4 \frac{(N \Delta T'_{\text{SUB}})^5}{\Delta T'_{\text{SUP}}^4}, \quad (6.1)$$

where N depends on the subcooling according to (4.15). When the subcooling is

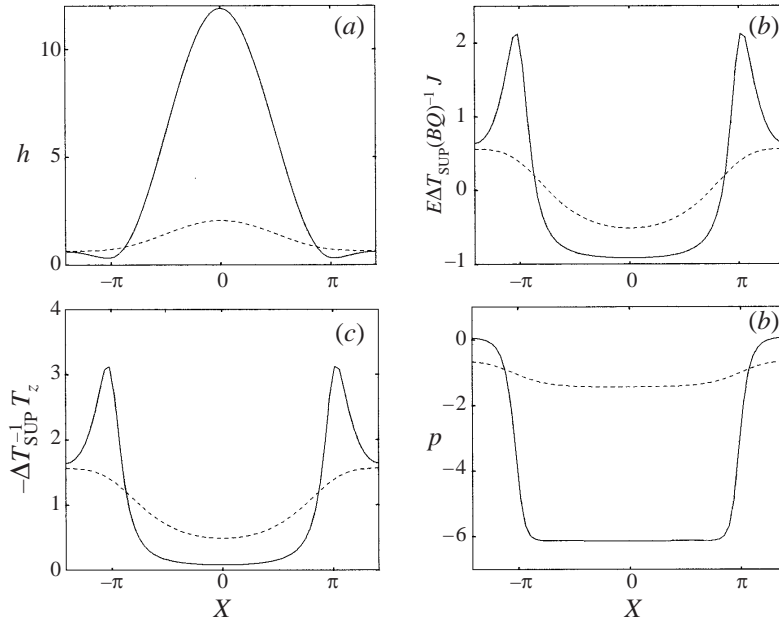


FIGURE 8. The dimensionless (a) film thickness, (b) mass flux, (c) heat flux and (d) pressure for two points on the bifurcation diagram of figure 7 when $\delta = 0.00434$, $A = 0$ and $H = 1$: ---, at the turning point; —, on the upper branch.

$\Delta T'_{\text{SUB}} = 15$ K, the neutrally-stable point corresponds to a superheat of $\Delta T'_{\text{SUP}} = 192.72$ K. For this particular value of the subcooling, $N = 1.7015$, and the heat transfer is enhanced by liquid convection. If the superheat is fixed, then an alternative form of the bifurcation diagram is obtained by varying the subcooling as shown in figure 7(c). The first and second turning points correspond to a subcooling of $\Delta T'_{\text{SUB}} = 14.991$ K and $\Delta T'_{\text{SUB}} = 15.020$ K, respectively. Since the temperature range between these turning points is only a fraction of a degree, the hysteresis loop would be difficult to observe unless the temperatures were very precisely controlled. If the subcooling is fixed and the superheat is varied, then another representation of the bifurcation diagram is obtained as shown in figure 7(d). In this case, the two turning points correspond to the superheats $\Delta T'_{\text{SUP}} = 192.92$ K and $\Delta T'_{\text{SUP}} = 192.26$ K, respectively. The temperature range between these two turning points is a bit larger. As a result, it would be easier to observe the hysteresis loop. As of yet, there is no experimental verification of this loop.

The solution at the first turning point along with the solution on the upper branch for the same value of δ is shown in figure 8 for the case $A = 0$. One could mentally divide the film profile into three regions: the large-amplitude vapour lobe in the middle, the surrounding thin film and the narrow transition region between the two, referred to as the gap region. Most of the evaporation takes place in the thin film, and the newly-generated vapour passes through the gap region, condensing in the vapour lobe. The net mass flux (found by integrating J over the entire interval) is zero because evaporation exactly balances condensation in equilibrium. Even though the film is stationary, there is a constant flow of vapour from the thin film into the vapour lobe.

The local mass flux is graphed in figure 8(b) for the corresponding film profiles in figure 8(a). Clearly, the maximum rate of evaporation occurs when the film thickness is

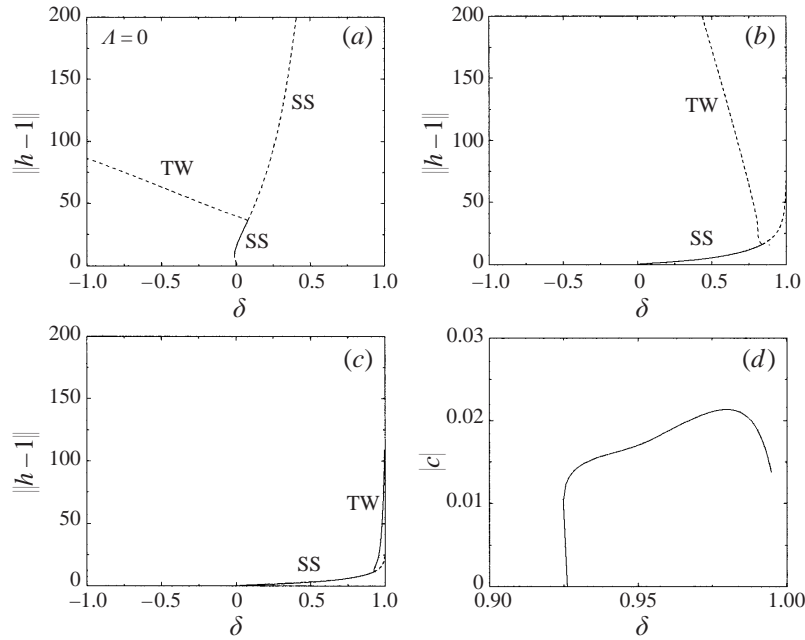


FIGURE 9. The steady-state (SS) and travelling-wave (TW) solutions of subcooled film boiling when $H = 1$: —, stable; ---, unstable. (a) $A = 0$; (b) $A = 0.3$; (c) $A = 0.5$; (d) wave speed c vs. δ along the stable TW branch in (c). There are 256 spectral modes.

a minimum. Note that as h gets larger, J approaches the constant rate of condensation $-BQ/E\Delta T_{\text{SUP}}H$ because the liquid-vapour interface gets further from the wall and the heat received from the solid is becoming negligible compared to the constant amount of heat being removed by the liquid subcooling. The net mass flux found by integrating (3.10) over one spatial period must be zero for a steady solution since, otherwise, the average film thickness would change with time.

The pressure shown in figure 8(d) is nearly constant everywhere except across the narrow gap region. From the normal-stress boundary condition (3.2), a constant-pressure solution corresponds to a sinusoidal film thickness. The sudden pressure drop across the gap is what drives the outward flow of vapour from the thin-film region. The characteristics of this pressure solution suggest that there might be a simpler way of representing the solution. That is, the film thickness can be thought of as consisting of two sinusoidal lobes joined together by the rapidly varying gap function. By focusing attention on the pressure boundary layer in the gap region, it might be possible to asymptotically match all three solutions together.

The effect of A on the bifurcation diagram is also shown in figure 7. As A increases, the critical value Q_C increases, and a larger subcooling is required to stabilize the basic state. At a critical value of A , the unstable solution branch disappears and the hysteresis loop is replaced by a single-valued branch of stable solutions.

There is a secondary bifurcation on the steady branch which gives rise to travelling waves with non-zero wave speed c . The steady solutions are unstable past this point. This is shown in figure 9 for three different values of A . When $A = 0$, the secondary bifurcation point is located at $\delta = 0.0778$. Symmetry requires each travelling wave to have a conjugate solution which is a reflected travelling wave moving in the opposite direction. For small enough A , this branch of travelling waves is subcritical

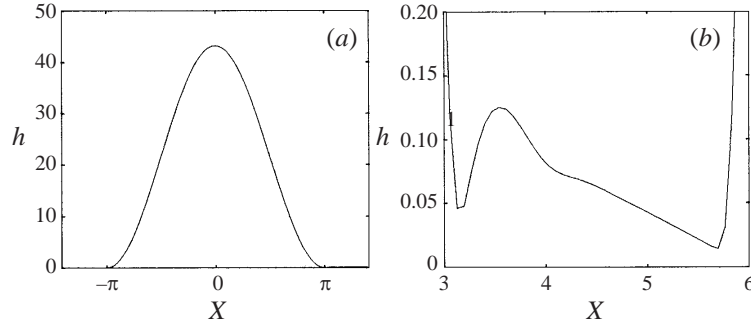


FIGURE 10. (a) Film profile of stable travelling wave in subcooled film boiling when $H = 1$, $A = 0.5$ and $\delta = 0.984$; (b) close-up of thin-film region. The wave moves to the right with speed $c = 0.0210$. There are 256 spectral modes.

and unstable as shown in figures 9(a) and 9(b). In this case, it appears that there are no stable solutions as δ is increased past the secondary bifurcation point. For sufficiently large A , the branch of travelling waves is supercritical and stable as shown in figure 9(c) for the particular value $A = 0.5$. The wave speed along this branch is shown in figure 9(d), and the film profile of a typical asymmetric travelling wave when $\delta = 0.984$ is shown in figure 10. The solution appears to be symmetric at first glance, but a closer look at the thin-film region clearly reveals the broken reflectional symmetry.

The secondary bifurcation point can be given in terms of the subcooling and superheat by using (6.1). For example, when $A = 0$ and with the dimensional subcooling fixed to $\Delta T'_{\text{SUB}} = 15$ K, the secondary bifurcation point at $\delta = 0.0778$ corresponds to $\Delta T'_{\text{SUP}} = 189.14$ K. Recall that for this particular subcooling the primary bifurcation from the basic state occurs when the superheat is $\Delta T'_{\text{SUP}} = 192.72$ K. Likewise, when the superheat is fixed to $\Delta T'_{\text{SUP}} = 192.72$ K, the secondary bifurcation occurs when $\Delta T'_{\text{SUB}} = 14.832$ K. Since the primary bifurcation point for this case occurs when the subcooling is $\Delta T'_{\text{SUB}} = 15$ K, the small temperature range separating these two bifurcation points would make it difficult, but not impossible, to observe the non-trivial steady solutions in experiments unless the temperatures were very precisely controlled. However, it would be better to fix the subcooling and vary the superheat because the temperature range between the bifurcation points is much larger. Increasing A moves the secondary bifurcation point further away from the primary bifurcation point as shown in figure 9. This would also make the bifurcated solutions easier to observe in the experiments.

6.2. Initial-value problems

6.2.1. Isothermal film (Rayleigh–Taylor instability)

If evaporative effects are neglected by choosing $Q = 0$, the vapour film approaches the steady solution

$$h(X) = \begin{cases} 0, & -\sqrt{2}\pi < X < -\pi \\ \sqrt{2}(1 + \cos X), & -\pi < X < \pi \\ 0, & \pi < X < \sqrt{2}\pi \end{cases} \quad (6.2)$$

in an infinite amount of time as shown by Yiantsios & Higgins (1989). This is supported by the numerical solution in figure 11(a). The basic state is unstable, and the film approaches the steady solution as expected, but it is never reached in any

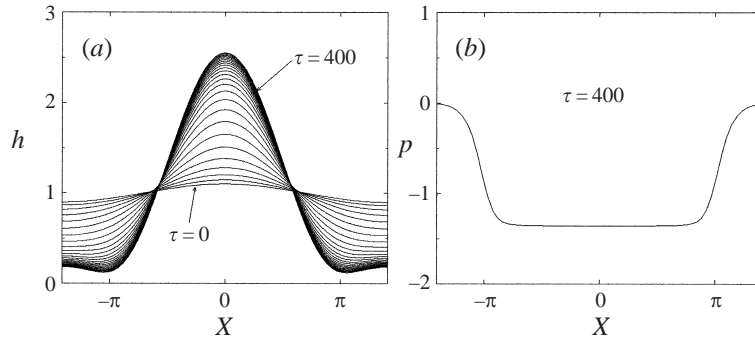


FIGURE 11. The collapse of an isothermal vapour film when $Q = 0$ due to the Rayleigh–Taylor instability: (a) film profile; (b) final pressure. The initial condition is $h = 1 + 0.1 \cos(X/\sqrt{2})$, timesteps are $\Delta\tau = 16$ and the solution is computed up to $\tau = 400$. The film approaches the steady solution given by (6.2). There are 256 spectral modes.

finite amount of time. A long-time asymptotic analysis by Hammond (1983) shows that the volume of the thin draining region between drops decays like $\tau^{-1/4}$ and that the minimum film thickness decays like $\tau^{-1/2}$. The final pressure shown in figure 11(b) is nearly constant everywhere except in the gap region.

6.2.2. Saturated film boiling

The saturated film-boiling limit is obtained as $H \rightarrow \infty$ with non-zero Q . In this case, the liquid is not cooled, the average film thickness increases with time and there are no steady solutions. A typical transient solution, which describes the initial growth of a vapour bubble, is shown in figure 12, assuming a perfectly conducting solid by choosing $A = 0$. The film volume increases at a nearly-constant rate as shown in figure 12(d), and most of this is accounted for by the rapidly-growing vapour lobe since the surrounding thin film is nearly stationary. It is apparent from figure 12(c) that the pressure is nearly constant in the vapour lobe and in the thin film but changes most rapidly across the gap region between them. Consequently, the maximum vapour velocity (and shear stress) is obtained within this region, and, thus, it is here that the validity of the long-wave equation may become questionable as previously mentioned in §3. However, as also previously noted in that same section, the numerical results for this case confirm that the pressure gradient still satisfies the validity condition for using the boundary condition $u = 0$ at $z = h$.

Most of the evaporation occurs in the nearly-stationary thin film, and the newly-generated vapour passes through the gap and into the vapour lobe. The minimum film thickness decays much more slowly compared to the isothermal case as shown in figure 12(f). Even though the thin film is nearly stationary when compared to the growing vapour lobe, a closer look at figure 12(b) uncovers some thickening on a much longer timescale.

Evaporative mass loss is stabilizing since it opposes the other mechanisms which act to collapse the film. When the film is isothermal, there is no evaporation and the minimum film thickness decays to zero. When evaporative effects are included and a perfectly conducting solid is assumed ($A = 0$), film collapse is suppressed. As the solid conductivity is decreased, A increases, and in the limit as $A \rightarrow \infty$, the solid is becoming such a poor conductor of heat that the solution approaches the isothermal case. This is because the evaporative term approaches the constant Q/A as $h \rightarrow 0$, so increasing A has the same effect as decreasing Q . Undoubtedly, there is a value

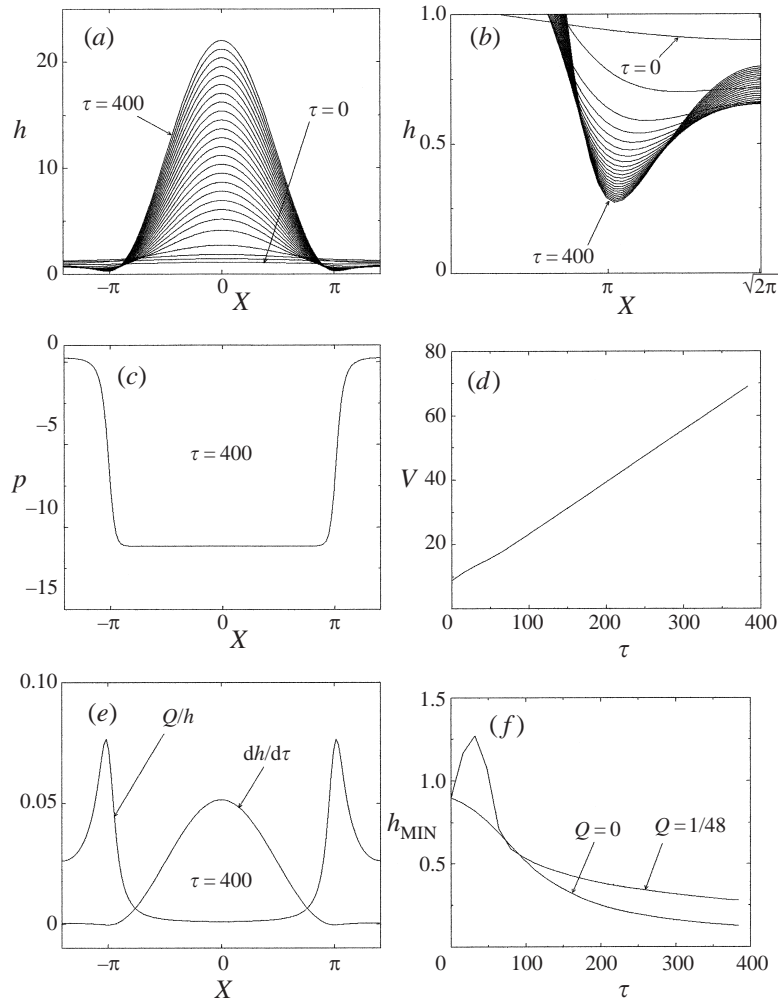


FIGURE 12. The growth of a vapour bubble during saturated film boiling when $H^{-1} = 0$, $A = 0$ and $Q = Q_C = 1/48$: (a) film profile; (b) close-up of the gap region; (c) final pressure; (d) film volume V ; (e) final interfacial velocity and mass flux; (f) minimum film thickness. The initial condition is $h = 1 + 0.1 \cos(X/\sqrt{2})$, the timesteps are $\Delta\tau = 16$ and the solution is computed up to $\tau = 400$. There are 256 spectral modes.

of A somewhere between the limiting values $A = 0$ and $A^{-1} = 0$ which just barely keeps the minimum film thickness out of the range of the intermolecular van der Waals forces so that the film will not collapse during the bubble-release cycle, and film boiling will persist.

Upon observing the pressure solution, it is clear that the pressure is nearly constant in the large and small lobes (with different constants) but is rapidly varying within the gap region. Thus, there is an internal pressure boundary layer in the gap. Since a constant-pressure solution corresponds to a sinusoidal film thickness, this suggests that it might be possible to find a simpler representation of the solution by asymptotically matching the two lobe solutions together through the pressure boundary layer in the gap. This was done by Hammond (1983) to find the draining time of the small lobe for the isothermal case.

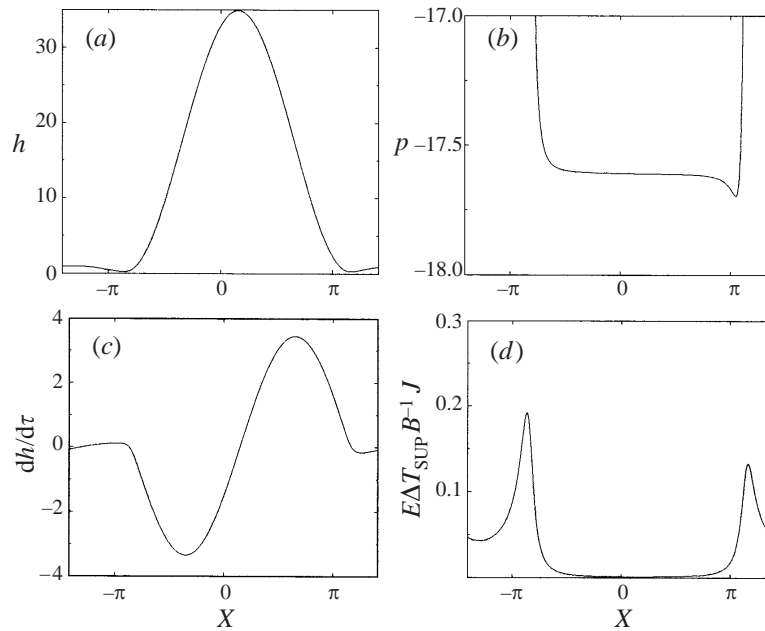


FIGURE 13. A travelling-wave solution that appears in saturated film boiling when $H^{-1} = 0$, $A = 0$ and $Q = 1/24$: (a) film profile; (b) pressure; (c) interfacial velocity; (d) evaporative mass flux. There are 256 spectral modes.

As time progresses, the symmetric solution is replaced by an asymmetric solution that has a travelling-wave character as shown in figure 13. It is not a permanent wave, however, because the average film thickness continues to increase, as it must for saturated film boiling. The broken symmetry moves the vapour lobe along the solid surface to the right or the conjugate solution to the left. Reflection about the vertical axis transforms one into the other. It is evident from figure 13 that the greater pressure on the upstream side is responsible for the flow downstream.

6.2.3. Subcooled film boiling

The stability of the subcooled basic state $h = 1$ is confirmed by solving an initial-value problem when $\delta = -0.05$ and $A = 0$. A slightly-perturbed film is attracted to the basic state as shown in figure 14(a). The basic state is unstable when $\delta > 0$, but figure 7 shows that there are two other stable solutions for each δ in the range $0 < \delta < 0.00434$. These solutions are locally attracting, but the global basin of attraction is unknown. Presumably, smaller-amplitude solutions are attracted to the lower branch while larger-amplitude solutions are attracted to the upper branch. This is partly confirmed by solving another initial-value problem when $\delta = 0.004$ and $A = 0$ as shown in figure 14(b). The instability of the basic state is confirmed, and the film approaches the smaller-amplitude solution predicted from the bifurcation diagram.

The time required to reach the subcooled steady state in figure 14(b) is much longer than the time required for similar growth during saturated film boiling (figure 12) or for the collapse of the isothermal film (figure 11). This is consistent with the experimental observation that subcooled film boiling usually progresses more slowly than the other boiling regimes (cf. Carey 1992).

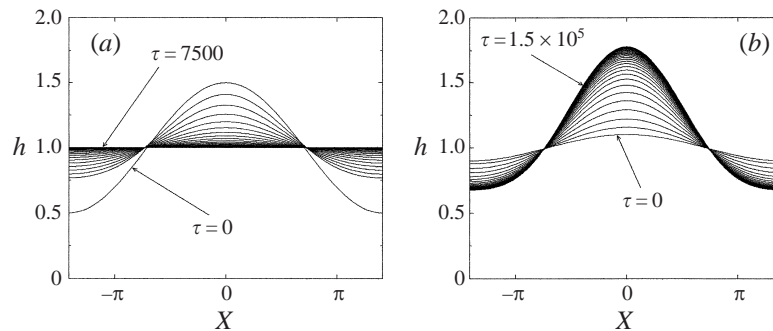


FIGURE 14. The vapour-film dynamics in subcooled film boiling when $H = 1$ and $A = 0$: (a) $\delta = -0.05$, initial condition is $h = 1 + 0.5 \cos(X/\sqrt{2})$, timesteps are $\Delta\tau = 250$; (b) $\delta = 0.004$, initial condition is $h = 1 + 0.1 \cos(X/\sqrt{2})$, timesteps are $\Delta\tau = 5000$. The solution in (a) converges to the basic state $h = 1$, confirming the linear-stability result, and the solution in (b) converges to the variable film thickness predicted by the bifurcation analysis. There are 256 spectral modes.

The growth of a vapour bubble in subcooled film boiling is shown in figure 15 when $\delta = 0.0045$ and $A = 0$. There is only one stable solution for this choice of parameters which lies on the upper branch of the bifurcation diagram in figure 7. The system starts near the basic state, and the film thickness increases in some places and decreases in others until it reaches this stable solution. The growth is not uniform, however, since the film volume increases very slowly at first but then increases rapidly before reaching the final equilibrium value as shown in figure 15(b). This non-uniform growth is understood by drawing an imaginary vertical line in figure 7 between the δ -axis and the point directly above it on the upper branch when $\delta = 0.0045$. Then, consider the state of the system as it evolves from the basic state to the steady solution to be associated with a point on this line which moves upwards as time increases. Since this line is just to the right of the turning point at $\delta = 0.0043$, the growth is slower as the system passes near the turning point. The growth is more uniform as δ is increased because the system does not pass so close to the turning point as it approaches the stable equilibrium.

The stable travelling-wave solution branch predicted from the bifurcation diagram in figure 9(c) is confirmed by solving an initial-value problem using the particular travelling-wave solution determined by AUTO as the initial condition. The numerical solution shown in figure 16 exhibits the expected wave behaviour, and the wave speed computed from the transient solution agrees with the wave speed computed by AUTO. The asymmetric film profile is evident in the close-up of the thin-film region shown in figure 16(b).

7. Conclusions

A long-wave evolution equation which describes film boiling is derived by determining the small Bond number limit (large surface tension) of the full liquid–vapour system of equations. The parameters are scaled so as to retain the most important effects of evaporation, surface tension and buoyancy in the final equation. A non-equilibrium evaporation condition and the thermal resistance of the solid plate are also included. The evolution equation proves to be a powerful tool for studying certain aspects of film boiling.

A constant-thickness vapour film is a solution in subcooled film boiling which

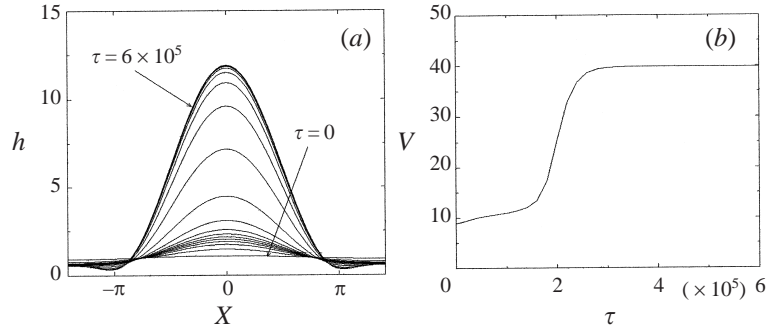


FIGURE 15. The growth of a vapour bubble in subcooled film boiling when $H = 1$, $\delta = 0.005$ and $\mathcal{A} = 0$: (a) film profile; (b) film volume. The initial condition is $h = 1 + 0.1 \cos(X/\sqrt{2})$, and the timesteps are $\Delta\tau = 2 \times 10^4$. The bubble growth is slow at first but speeds up rapidly before approaching the stable steady solution. There are 256 spectral modes.

exactly balances the heat received from the solid wall with the heat loss due to liquid subcooling. This is stable if $Q > Q_C$, and since Q is proportional to the subcooling, a sufficiently large subcooling (with fixed superheat) will stabilize this basic state as shown in figure 5(a). For example, when $\mathcal{A} = 0$ and using the typical material properties in table 1 with a fixed subcooling of $\Delta T'_{\text{SUB}} = 15$ K, the basic state is stable if the superheat is less than $\Delta T'_{\text{SUP}} = 192.72$ K. Likewise, when the superheat is fixed to $\Delta T'_{\text{SUP}} = 192.72$ K, the basic state is stable when the subcooling is greater than $\Delta T'_{\text{SUB}} = 15$ K. Since increasing the subcooling with the superheat fixed decreases the equilibrium film thickness, the film is stable if it is thin enough.

Another important observation is that it would be much easier to observe the equilibrium film in microgravity because the destabilizing force of gravity is reduced. To see this, note that the critical film thickness is inversely proportional to the square of the gravitational acceleration, $d_C \propto g^{-2}$. If all the other parameters were held fixed as the strength of gravity is reduced, the critical film thickness would increase, and a stable, constant-thickness film would be observed with a much greater thickness than is possible on the ground. Perhaps, future Space experiments could be designed to validate or discount some of the results presented here.

A weakly-nonlinear analysis reveals a supercritical bifurcation at the point $Q = Q_C$. In terms of $\delta = 1 - Q/Q_C$, linear theory shows the basic state is stable if $\delta < 0$ and unstable if $\delta > 0$. The film profile corresponding to the branching solutions is, at leading order in δ , a sinusoidal modulation of the basic state.

The numerical bifurcation package AUTO is then used to follow the solution branches into the strongly-nonlinear regime. The branch bends back and forms a hysteresis loop if \mathcal{A} is small enough as shown in figure 7. Physically, when $\mathcal{A} = 0$, this means that as the subcooling is decreased with the superheat fixed to $\Delta T'_{\text{SUP}} = 192.72$ K, there is a continuous transition to a non-uniform film thickness at $\Delta T'_{\text{SUB}} = 15$ K and then a jump transition to a large-amplitude solution (upper branch) when the subcooling is decreased below the first turning point at $\Delta T'_{\text{SUB}} = 14.991$ K. If the subcooling were then increased again, the system would move along the upper branch in the opposite direction, and the film thickness would gradually decrease until the second turning point at $\Delta T'_{\text{SUB}} = 15.020$ K is passed, at which time the system would immediately drop back down to the basic state. If, on the other hand, the subcooling is decreased while on the upper branch, the steady branch loses stability to a branch of travelling waves at $\Delta T'_{\text{SUB}} = 14.832$ K as shown in figure 9. The branch of travelling

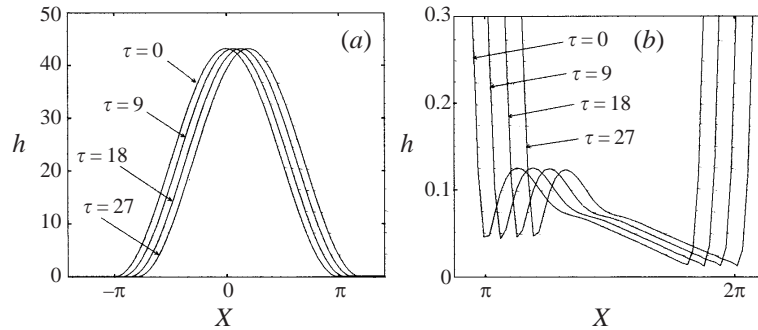


FIGURE 16. A stable travelling-wave solution that appears during subcooled film boiling when $H = 1$, $A = 0.5$ and $\delta = 0.984$: (a) entire film profile; (b) close-up of thin-film region. The initial condition is the travelling-wave solution computed by AUTO, and the timesteps are $\Delta\tau = 9$. This wave moves to the right with a wave speed that agrees with the value $c = 0.021$ computed by AUTO. There are 256 spectral modes.

waves is subcritical and unstable for small A but supercritical and stable for large enough A . An analogous behaviour is observed when the subcooling is fixed and the superheat is varied. As A gets larger, the hysteresis loop vanishes and is replaced by a single-valued branch of steady solutions.

One must observe a bit of caution. Travelling waves are predicted here in a model that is spatially periodic. If in an experiment such conditions were valid, then these waves would be observable. However, in other cases, the edge conditions might preclude their existence. For example, one situation which might exhibit this behaviour is film boiling on the interior surface of a large-diameter pipe in microgravity which is spinning about its axis. The subcooling could be provided by inserting another smaller-diameter pipe carrying cooler liquid along the axis of the larger pipe. The centrifugal force due to the spinning pipe would be analogous to gravity, but it would always be directed radially outwards. Then, the circular symmetry of the pipe would introduce periodic boundary conditions in the circumferential direction.

In saturated film boiling, there are no equilibrium solutions because there is no liquid subcooling, but a direct numerical solution of the evolution equation is used to study the formation of a vapour bubble during the early and intermediate stages of growth. A number of important characteristics of this process are uncovered. Namely, the pressure is nearly constant in the growing vapour lobe and in the surrounding thin film but changes rapidly across the narrow gap region connecting them. This suggests that it might be possible to derive a simpler representation of the solution by asymptotically matching the two sinusoidal solutions through the pressure boundary layer in the gap. In addition, the film volume increases at a nearly-constant rate, but most of this growth is accounted for by the expanding vapour lobe since the thin-film region is relatively motionless. The bulk of the evaporation occurs in the nearly-stationary thin film, and the newly-generated vapour is transported through the gap region into the growing vapour lobe. This is an important observation because it indicates that the dynamics of vapour-bubble growth are dictated by what happens in the thin-film and gap regions, and the growing vapour lobe is mainly a repository of newly-generated vapour. The thin-film is quasi-steady because there is a local balance between evaporation and the outward flow of vapour.

One of the goals of film-boiling research is to predict the minimum superheat required to sustain film boiling. It is known that this depends not only on the

temperature of the solid but also on other surface properties such as the liquid–solid contact angle and the surface roughness (cf. Witte & Lienhard 1982). The present paper does not consider the effects of liquid–solid contact but rather the dynamics which might lead to such contact. It is seen that evaporation has a stabilizing effect, and a local equilibrium thickness is maintained which balances evaporation with the other mechanisms acting to collapse the film as shown in figure 12(*f*). When the film is isothermal, there is no evaporation, and the minimum film thickness decays to zero. However, when evaporative effects are included and a perfectly-conducting solid is assumed ($A = 0$), the minimum thickness decays more slowly and even appears to be approaching a non-zero constant.

Two effects not included in the present evolution equation are the van der Waals intermolecular forces and *vapour thrust*, the pressure jump across the free surface due to the recoil of evaporating molecules. These effects are usually retained in the evolution equations which describe thin liquid films (cf. Buelbach *et al.* 1988), but they are usually negligible in film boiling unless the film gets very thin. To make this statement explicit, consider the evolution equation for saturated film boiling that would result if these effects were retained,

$$h_\tau = \frac{Q}{h} - \frac{1}{12} \left[h^3 h_X + h^3 h_{XXX} - 2GB^2 Q^2 h_X + 3A \frac{h_X}{h} \right]_X, \quad (7.1)$$

where $G = \rho \Delta \rho g d^3 / \mu^2$ is the Reynolds number in the vapour, and $A = A' / (6\pi \Delta \rho g d^4)$ is the dimensionless Hamaker constant which measures the relative strength of the molecular attractions (cf. Panzarella 1998). Next, each effect is compared to buoyancy, the driving mechanism behind the instability. The ratio of the vapour thrust term to the buoyancy term is

$$\frac{\text{vapour thrust term}}{\text{buoyancy term}} = 2GB^2 Q^2 \frac{1}{h^3}. \quad (7.2)$$

Likewise, the ratio of the van der Waals term to the buoyancy term is

$$\frac{\text{van der Waals term}}{\text{buoyancy term}} = 3A \frac{1}{h^4}. \quad (7.3)$$

These ratios are graphed in figure 17 along with an indication of the minimum film thickness observed in the numerical solution shown in figure 12. The parameter values are taken from table 1. It is seen that these terms are negligible unless the film thickness gets very small. Since the minimum film thickness never gets small enough for these other effects to become important, it is reasonable to neglect them in the present analysis. A boundary element analysis is used in Panzarella (1998) to extend these solutions up to the point of bubble detachment, and it is shown that the film thickness never drops below a minimum value which is outside the range of these forces. The thin liquid film considered by Buelbach *et al.* (1988) had an average thickness of about $d = 10^{-6}$ cm, which corresponds to $h = 10^{-4}$ in the current problem. In that case, the vapour thrust and van der Waals attractions are not only important but dominate over buoyancy. For this reason, buoyancy was neglected in their problem, but it must be considered here.

As with any asymptotic solution, it is always useful to check that the terms which were neglected are indeed small. This shows whether the leading-order solution is consistent or not. In the current example, one of the major assumptions is that the convective terms in the horizontal momentum equation are negligible when compared

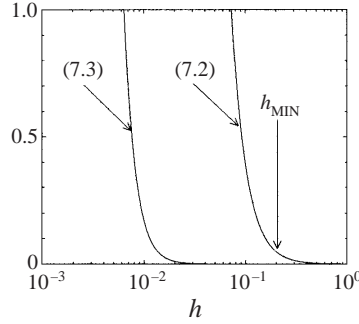


FIGURE 17. The ratio of vapour thrust to buoyancy terms given by (7.2) and the ratio of van der Waals to buoyancy terms given by (7.3) using the parameter values listed in table 1. These effects only become important when h gets very small. Also indicated in the graph is h_{MIN} , the minimum film thickness observed in the numerical solution of figure 12, which is outside the range where these other effects become comparable to buoyancy. This justifies the absence of these additional terms in the leading-order evolution equation.

to the dominant viscous terms. This explicitly requires $Gu_t \ll u_{zz}$, $Guu_x \ll u_{zz}$ and $Gwu_z \ll u_{zz}$. The leading-order horizontal and vertical velocity components are

$$u = \frac{1}{2}z(h-z)(h+B^{-1}h_{xx})_x, \quad (7.4)$$

$$w = \frac{1}{12}[z^2(2z-3h)(h+B^{-1}h_{xx})]_x. \quad (7.5)$$

Since the maximum vapour velocity is attained near the minimum film thickness point, this would be the most likely place for the convective terms to become important. At the minimum film thickness point, the slope is zero ($h_x = 0$). Only saturated film boiling will be considered. The numerical solution in figure 12 shows that the solution is quasi-steady in the thin film surrounding the growing vapour lobe. That is, the film profile does not change much because there is a local balance between evaporation and the flow of vapour out of the film. This is expressed by the equation

$$\frac{QB}{h} = \frac{1}{12}[h^3(h_x+B^{-1}h_{xxx})]_x. \quad (7.6)$$

By assuming the local balance expressed by (7.6) and using (7.4) and (7.5), it is possible to show that the convective terms are negligible as long as

$$GQB \ll 1. \quad (7.7)$$

As it should be, the previous condition is independent of the initial film thickness d . For the particular material properties and parameter values in table 1, $GQB = 0.08$. Thus, it is reasonable to neglect the convective terms, and the leading-order solution represented by the evolution equation is consistent. In saturated film boiling, Q is linearly proportional to the superheat. Thus, the convective terms become more important as the superheat is increased.

This paper only considers two-dimensional disturbances with $h = h(x, t)$. A three-dimensional model would require $h = h(x, y, t)$, where y is the other horizontal coordinate. This would be a very useful extension of the current work because most, if not all, film-boiling experiments exhibit three-dimensional behaviour. A more quantitative prediction of bubble shape and size would be possible using the three-

dimensional evolution equation. The one-dimensional evolution equation can be easily extended to two dimensions with the result

$$h_\tau = Q \frac{1 - h/H}{h + A} - \frac{1}{12} \nabla \cdot [h^3 \nabla h + h^3 \nabla (\nabla^2 h)], \quad (7.8)$$

where ∇ is the gradient operator with respect to the scaled coordinates $X = B^{1/2}x$ and $Y = B^{1/2}y$.

This work was supported by a fellowship from the Defense Advanced Research Projects Agency, Department of Defense as well as a grant from the Engineering Research Program of the Office of Basic Sciences, Department of Energy.

REFERENCES

- ABBASSI, A. & WINTERTON, R. H. S. 1989 The non-boiling vapour film. *Intl J. Heat Mass Transfer* **32**, 1649–1655.
- ASTON, P. J., SPENCE, A. & WU, W. 1992 Bifurcation to rotating waves in equations with O(2)-symmetry. *SIAM J. Appl. Maths* **52**, 792–809.
- BERENSON, P. J. 1961 Film boiling heat transfer from a horizontal surface. *J. Heat Transfer* **83**, 351.
- BURELBACH, J. P., BANKOFF, S. G. & DAVIS, S. H. 1988 Nonlinear stability of evaporating/condensing liquid films. *J. Fluid Mech.* **195**, 463–494.
- CAREY, VAN P. 1992 *Liquid-Vapour Phase-Change Phenomena*. Hemisphere.
- CHANG, Y. P. 1959 Wave theory of heat transfer in film boiling. *J. Heat Transfer* **81**, 112.
- DELHAYE, J. M. 1974 Jump conditions and entropy sources in two-phase systems. *Intl J. Multiphase Flow* **1**, 395–409.
- DOEDEL, E. J. 1981 AUTO, a program for the automatic bifurcation analysis of autonomous systems. *Congressus Numerantium* **30**, 265.
- ERVIN, J. S., MERTE, H., JR., KELLER, R. B., KIRK, K. 1992 Transient pool boiling in microgravity. *Intl J. Heat Mass Transfer* **35**, 659–674.
- HAMMOND, P. S. 1983 Nonlinear adjustment of a thin annular film of viscous fluid surrounding a thread of another within a circular cylindrical pipe. *J. Fluid Mech.* **137**, 363–384.
- HOLLANDS, K. G. T., RAITHBY, G. D. & KONICEK, L. 1975 Correlation equations for free convection heat transfer in horizontal layers of air and water. *Intl. J. Heat Mass Transfer* **18**, 879–884.
- KIKUCHI, Y., EBISU, T. & MICHIOYOSHI, I. 1992 Measurement of liquid-solid contact in film boiling. *Intl J. Heat Mass Transfer* **35**, 1589–1594.
- ORON, A., BANKOFF, S. G. & DAVIS, S. H. 1996 Thermal singularities in film rupture. *Phys. Fluids* **8**, 3433–3435.
- ORON, A., DAVIS, S. H. & BANKOFF, S. G. 1997 Long-scale evolution of thin liquid films. *Rev. Mod. Phys.* **69**, 931–980.
- PALMER, H. J. 1976 The hydrodynamic stability of rapidly evaporating liquids at reduced pressure. *J. Fluid Mech.* **75**, 487–511.
- PANZARELLA, C. H. 1998 Nonlinear Analysis of Horizontal Film Boiling. PhD Thesis, Department of Engineering Sciences and Applied Mathematics, Northwestern University.
- PETZOLD, L. R. 1983 Automatic selection of methods for solving stiff and nonstiff systems of ordinary differential equations. *SIAM J. Sci. Statist. Comput.* **4**, 136–148.
- SCHRAGE, R. W. 1953 *A Theoretical Study of Interphase Mass Transfer*. Columbia University Press, New York.
- SHOJI, M. & KANEKO, Y. 1986 Film boiling and minimum heat flux of saturated pool boiling on a horizontal surface. *Proc. 23rd National Heat Transfer Symposium of Japan*, pp. 220–222.
- TANAKA, H. 1988 On the stability of vapour film in pool film boiling. *Intl J. Heat Mass Transfer* **31**, 129–134.
- WILLIAMS, M. B. & DAVIS, S. H. 1982 Nonlinear theory of film rupture. *J. Colloid Interface Sci.* **90**, 220–228.

- WITTE, L. C. & LIENHARD, J. H. 1982 On the existence of two “transition” boiling curves. *Intl J. Heat Mass Transfer* **25**, 771–779.
- YIANTSIOS, S. G. & HIGGINS, B. G. 1989 Rayleigh–Taylor instability in thin viscous films. *Phys. Fluids A* **1**, 1484–1501.
- ZUBER, N. 1959 Hydrodynamic aspects of boiling heat transfer. *AEC Rep.* AECU-4439. June.